Article

99mTc-Labeled RGD-Polyethylenimine Conjugates with Entrapped Gold Nanoparticles in the Cavities for Dual Mode SPECT/CT Imaging of Hepatic Carcinoma

Benqing Zhou, Ruizhi Wang, Feng Chen, Lingzhou Zhao, Peng Wang, Xin Li, István Bányai, Qiang Ouyang, Xiangyang Shi, and Mingwu Shen

Just Accepted

^{99m}Tc-Labeled RGD-Polyethylenimine Conjugates with Entrapped Gold Nanoparticles in the Cavities for Dual Mode SPECT/CT Imaging of Hepatic Carcinoma

Benqing Zhou[a,1], Ruizhi Wang[b,1], Feng Chen [a], Lingzhou Zhao[c], Peng Wang[a], Xin Li[a], István Bányai,[d]* Qiang Ouyang[b]*, Xiangyang Shi[a], and Mingwu Shen[a]*

[a] State Key Laboratory for Modifcation of Chemical Fibers and Polymer Materials, College of Chemistry, Chemical Engineering and Biotechnology, Donghua University, Shanghai 201620, P. R. China

[b] Department of interventional radiology, Xinhua hospital affiliated to Shanghai Jiaotong University, Shanghai 200080, P. R. China

[c] Department of Nuclear Medicine, Shanghai General Hospital, School of Medicine, Shanghai Jiaotong University, Shanghai 200080, P. R. China

[d] Department of Physical Chemistry, University of Debrecen, Debrecen, Hungary

Keywords: gold nanoparticles; ^{99m}Tc; polyethylenimine; SPECT/CT imaging; hepatic carcinoma

_____

* Corresponding author. E-mail address: mwshen@dhu.edu.cn (M. Shen), ouyangqiang@aliyun.com (Q. Ouyang), and banyai.istvan@science.unideb.hu (I. Banyai)

[1] Authors contributed equally to this work.

Abstract

We report the construction and characterization of ^{99m}Tc-labeled arginine-glycine-aspartic acid (RGD)-polyethylenimine (PEI) conjugates with entrapped gold nanoparticles in the cavities (RGD-^{99m}Tc-Au PENPs) for dual mode SPECT/CT imaging of an orthotopic hepatic carcinoma model. In this study, PEI was successively decorated with diethylenetriaminepentaacetic acid, polyethylene glycol (PEG), and PEGylated RGD segments, and was utilized as an effective nanoplatform to entrap Au NPs and to be labelled with ^{99m}Tc. We show that the designed RGD-^{99m}Tc-Au PENPs display desirable colloidal stability and radiostability, and cytocompatibility in the investigated concentration range, and can be specifically uptaken by $\alpha_v\beta_3$ integrin-overexpressing liver cancer cells *in vitro*. *In vivo* CT and SPECT imaging results indicate that the particles are able to be accumulated within an orthotopic hepatic carcinoma and display both CT and SPECT contrast enhancement in the tumor tissue. With the proven biocompatibility *in vivo via* histological examinations, the designed RGD-^{99m}Tc-Au PENPs may be potentially employed as an effective nanoprobe for highly efficient dual mode SPECT/CT imaging of various $\alpha_v\beta_3$ integrin-overexpressing tumors.

Introduction

Hepatic carcinoma has been regarded as the 5th common type of cancer and 3rd common cancer-related deaths over the world, and it usually evolves from chronic liver disease.[1-3] Imaging modalities for diagnosis of hepatic carcinoma mainly include ultrasonography,[4-5] magnetic resonance (MR) imaging,[6-7] computed tomography (CT)[8] and nuclear imaging (e.g., single-photon emission computed tomography (SPECT)[9-10] and positron emission tomography (PET)[11]). Development of effective contrast agents allowing for single mode or multi-mode diagnostic imaging is generally required to achieve precision imaging performances.

Thanks to the unique structures and properties, nanoparticles (NPs) have been applied in different biomedical fields.[12-13] Among these applications, NP-based contrast agents have been designed for CT,[14-15] MR,[16-18] SPECT[19-20] and fluorescence imaging[21-22] *etc.* in order to improve the resolution and sensitivity of these imaging modes. For instance, polyethylene glycol (PEG)-stabilized gold NPs (Au NPs, ~30 nm of diameter) were prepared and used as a contrast agent for effective blood pool/liver CT imaging.[23] Au NPs having a diameter of 5 nm can be decorated with a peptide and doped with ^{199}Au for targeted tumor SPECT imaging.[24] Nevertheless, each imaging mode possesses its intrinsic virtues and drawbacks. CT imaging as a structural imaging mode can make a reconstruction of three-dimensional tomography with a high spatial resolution, but falls behind with poor soft-tissue contrast.[25] In contrast, SPECT or PET imaging as a functional imaging mode displays a high sensitivity, along with an ability to trace *in vivo* particle biodistribution in real time,[26] whereas it lacks spatial resolution. Therefore, to further improve the accuracy and sensitivity of tumor diagnosis, it is reasonable to make use of the strengths of both structural and functional imaging modalities by combining two or more imaging elements in one platform to fabricate dual- or multi-modality contrast agents.

According to the literature reports, arginine-glycine-aspartic acid (RGD) peptide-targeted Au NPs loaded with gadolinium (Gd) and labeled with ^{99m}Tc (RGD@AuNPs-Gd^{99m}Tc) can be prepared with different sizes (29, 51, or 80 nm) for targeted MR/SPECT dual mode imaging-guided

radiosensitization therapy of tumor angiogenesis.[27] RGD-conjugated ^{99m}Tc-labeled Au NPs (diameter = 20 nm) *via* a spontaneous reaction of the thiol group have been designed for tumor SPECT/CT imaging applications.[28] Citrated-coated [^{64}Cu]CuS NPs with a diameter of 11 nm can be modified with PEG to have a good stability for micro-PET/CT dual mode imaging and photothermal therapy of tumors due to their strong near-infrared absorption peak at 930 nm.[29] Moreover, it is well documented that tumor uptake of particles through the passive enhanced permeability and retention (EPR) effect is less efficient than that through active targeting. Hence, active targeting is inevitable to acquire better resolution of diagnostic imaging.[30-34] However, it is still challengeable to develop such multifunctional NPs with two or more imaging elements incorporated and functional moieties such as targeting ligands modified on the same NP systems. The key factor is to use a proper platform which facilitates conjugation, encapsulation or stabilization of the imaging element and modification of functional groups on the surface of NPs.

Branched polyethylenimine (PEI), having abundant amines and good water solubility, has been widely used as a nanoplatform to coat NPs or load drug molecules for different biomedical applications.[35-39] In our previous study, we demonstrate that PEI can be used as a template to entrap Au NPs for CT imaging,[40-42] or be used as a stabilizer to coat the surface of iron oxide (or manganese oxide) NPs for MR imaging.[43-45] It is logical to speculate that PEI may serve as a versatile nanoplatform to load both Au NPs (for CT imaging) and ^{99m}Tc (for SPECT imaging) for dual mode SPECT/CT imaging of hepatic carcinoma.

The aim of the current work was to fabricate RGD peptide-targeted PEI-entrapped Au NPs labeled with ^{99m}Tc (RGD-^{99m}Tc-Au PENPs) for highly efficient SPECT/CT imaging of an orthotopic hepatic carcinoma model. We prepared the multifunctional RGD-^{99m}Tc-Au PENPs and fully characterize them by means of different techniques. Cell counting kit-8 (CCK-8) assay and confocal microscopic imaging of cell morphology were used to assess the cytotoxicity of the particles. HCC-LM3 cells (a human hematoma cell line) overexpressing $\alpha_v\beta_3$ integrin were utilized to confirm the specific targeting property of the RGD-conjugated nanoprobes *in vitro*. *In vivo* CT and SPECT imaging were utilized to check their potential to be employed for efficient SPECT/CT imaging of an

4

orthotopic human hepatic carcinoma model. A thorough literature investigation leads us to claim that this is the very first trial dealing with the preparation of RGD-functionalized and ^{99m}Tc-labeled Au PENPs for dual mode SPECT/CT imaging of tumors.

Experimental Section

Synthesis of PEI.NH$_2$-DTPA-mPEG-(PEG-RGD). RGD-PEG-COOH was prepared in line with the literature.[46] To prepare the PEI.NH$_2$-DTPA-mPEG-(PEG-RGD) conjugate, DTPA (7.14 mg, 5 mL DMSO) was added into a PEI DMSO solution (50 mg, 10 mL) under stirring for 1 day. Afterwards, mPEG-COOH (80 mg, 8 mL DMSO) was activated by 76.7 mg of 1-ethyl-3-(3-dimethylaminopropy) carbodiimide hydrochloride (EDC) and 46.0 mg of N-hydroxysuccinimide (NHS) and added to the above PEI.NH$_2$-DTPA solution, and then the above solution was magnetically stirred for another 3 days to obtain the raw product of PEI.NH$_2$-DTPA-mPEG. Lastly, the EDC/NHS-activated RGD-PEG-COOH (51 mg, 7 mL DMSO) was added to the above PEI.NH$_2$-DTPA-mPEG solution under stirring for 3 days. The prepared PEI.NH$_2$-DTPA-mPEG-(PEG-RGD) mixture was purified by dialysis and lyophilized to get a powder in accordance with our previous work.[42]

Synthesis of RGD-^{99m}Tc-Au PENPs. The formed PEI.NH$_2$-DTPA-mPEG-(PEG-RGD) was used as an effective template for the entrapment of Au NPs. In brief, HAuCl$_4$ (10 mg/mL, in 8.24 mL water) with 200 molar equiv. of PEI.NH$_2$-DTPA-mPEG-(PEG-RGD) was firstly added slowly to the PEI.NH$_2$-DTPA-mPEG-(PEG-RGD) water solution (76.9 mg, 200 mL) with vigorous stirring for about 15 min. Then, the icy NaBH$_4$ (4.7 mg, 5 mL) water solution was quickly dropped into the above Au(III) salt/PEI.NH$_2$-DTPA-mPEG-(PEG-RGD) mixture solution, followed by continuous agitation for 3 h. The formed {(Au^0)$_{200}$-PEI.NH$_2$-DTPA-mPEG-(PEG-RGD)} was acetylated to prepare {(Au^0)$_{200}$-PEI.NHAc-DTPA-mPEG-(PEG-RGD)} PENPs (for short, RGD-Au PENPs) according to the literature.[42] The mixture was then purified in line with our previous work.[42]

The formed RGD-Au PENPs were then labeled with ^{99m}Tc through DTPA chelation. In brief, the RGD-Au PENPs solution (1 mg/mL, in 3 mL PBS) was initially added into an SnCl$_2$ PBS solution

(50 mg/mL, 2 mL) under stirring for 8 min, and then sterile TcO_4^- salt (700 MBq/mL, 1 mL) was added under stirring for another 5 min. Lastly, the formed {$(Au^0)_{200}$-PEI.NHAc-DTPA(^{99m}Tc)-mPEG-(PEG-RGD) PENPs (for short, RGD-^{99m}Tc-Au PENPs) was purified using PD-10 desalting columns according to our previous work.[47]

Cytotoxicity Assays. We used standard CCK-8 assay method to test the cytocompatibility of the particles reported in the literature.[48] Similarly, HCC-LM3 cells were cocultured with the RGD-Au PENPs ([Au] = 0-200 μM) for 24 h, followed by rinsing with PBS, paraformaldehyde fixation, and 4',6-diamidino-2-phenylindole (DAPI) staining. The cell morphology was viewed under a Leica DM IL LED inverted phase contrast microscope (Wetzlar, Germany). To check how the particles impacted on the cytoskeleton, HCC-LM3 cells were seeded on cover slips in a 12-well plate with 1 mL of fresh Dulbecco's modified Eagle medium (DMEM) for each well for 12 h. The cells were treated using protocols in our previous work[49] before confocal microscopic observation.

Cell Immunohistochemistry. 5×10^4 HCC-LM3 cells and L929 cells (a mouse fibroblast cell line, as negative control cells) were cultured onto each cover slip in a 12-well plate with 1 mL of fresh DMEM for each well for 24 h, respectively. After being washed twice and fixed, the cells were rinsed 3 times and treated with 3% H_2O_2 for 15 min. After that, the cells in each well were washed, added with 300 μL of immunostaining mounting medium, and incubated for another 20 min. Next, the mounting medium was carefully removed, and primary $\alpha_v\beta_3$ integrin antibody (mouse anti-human, 1: 200) was added to each well, and the cells were cultured overnight in dark at 4 ^{o}C. Hereafter, the cells were washed with PBS for three times, and incubated with red fluorescent AF594-labeled secondary antibody (goat anti-mouse, 1:200) for 1 h at 37 ^{o}C in dark. Finally, the cells were rinsed and stained with DAPI for 10 min before confocal microscopic imaging. These L929 cells and HCC-LM3 cells were both treated with or without primary antibody, respectively.

CT Imaging of an Orthotopic Hepatic Carcinoma Model *in Vivo*. Animal experiments were performed following both requirements of the institutional committee for animal care and the National Ministry of Health. Both nude mice and C57BL/6 mice were purchased from Shanghai

6

SLAC Laboratory Animal Center (Shanghai, China). An orthotopic hepatic carcinoma model was established on nude mice according to our previous protocol.[50] In brief, 5×10^6 HCC-LM3 cells were first subcutaneously injected into the right flank of each nude mouse (6-week-old) to establish a subcutaneous HCC-LM3 tumor transplantation model. The tumor was extracted after its volume reaches up to 200-300 mm^3. Then, the tumor was cut into small pieces with a dimension of 1 mm^3, and planted into the liver of each nude mouse to establish an orthotopic hepatic carcinoma model. We then intravenously injected the RGD-Au PENPs or Au PENPs ([Au] = 0.1 M, in 150 μL PBS) to each tumor-bearing mouse *via* tail vein after the mouse was anesthetized. The mice were then put into a CT scanning holder, and scanning was then performed according to the literature.[40]

SPECT/CT Imaging of an Orthotopic Hepatic Carcinoma Model *in Vivo*. The synthesized RGD-^{99m}Tc-Au PENPs or nontargeted ^{99m}Tc-Au PENPs (600 μCi ^{99m}Tc, in 150 μL PBS) were intravenously delivered to each mouse after anesthetization. Then, the mice were scanned by a SPECT/CT imaging system using a Nano SPECT/CT in Vivo Animal Imager (Bioscan Ltd., Washington, D.C.) with 80 kV, 450 μA and slice thickness of 45 μm.

Results and Discussion

Construction and Characterization of the RGD-^{99m}Tc-Au PENPs. DTPA, *m*PEG-COOH, and RGD-PEG-COOH were successively modified onto the PEI surface to synthesize PEI.NH$_2$-DTPA-*m*PEG-(PEG-RGD). Then the PEI.NH$_2$-DTPA-*m*PEG-(PEG-RGD) was employed as a desirable nanoreactor to entrap Au NPs, and the formed Au PENPs were acetylated to neutralize the remaining PEI amines and chelated with ^{99m}Tc (Scheme 1). The prepared RGD-Au PENPs and RGD-^{99m}Tc-Au PENPs were characterized through various techniques.

Firstly, the structures of the RGD-PEG-COOH, PEI.NH$_2$-DTPA, PEI.NH$_2$-DTPA-*m*PEG-(PEG-RGD), and RGD-Au PENPs were characterized *via* NMR (Figure S1, Supporting Information). The peaks at 3.5-3.6 ppm belong to -CH$_2$- protons of PEG, and 5.8-7.3 ppm to the benzene ring of RGD protons (Figure S1a). According to the NMR peak integration, each

PEG was estimated to have 0.78 RGD moieties linked. Likewise, NMR integration shows that each PEI (δ: 2.2-3.5 ppm) has 9.5 DTPA (δ: 3.0-3.4 ppm), 22.4 PEG, and 5.2 RGD moieties linked (Figure S1b-c). After the remaining amines of RGD-Au PENPs were acetylated, the peaks of acetyl protons located at 1.8-2.2 ppm appears (Figure S1d), which can be assigned to the primary and secondary PEI amides.[41]
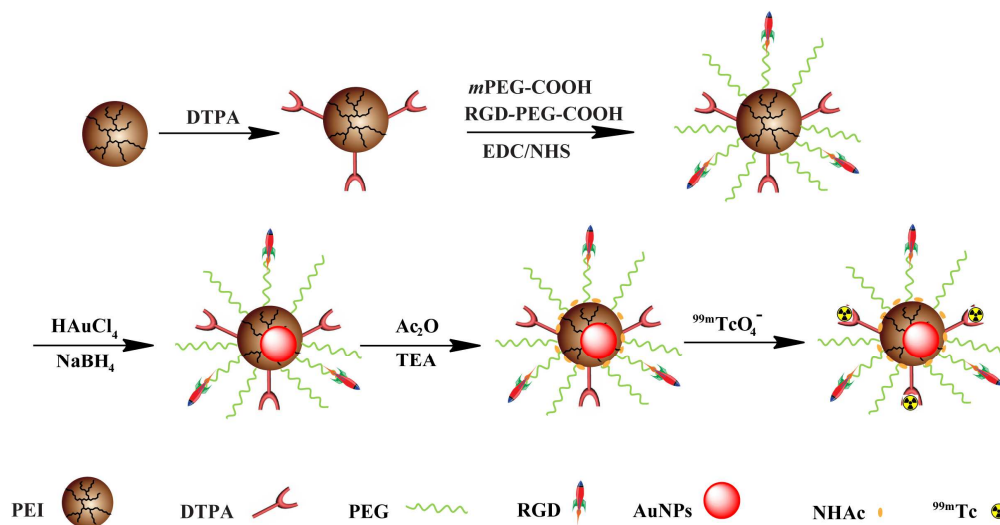
Scheme 1. Schematic diagram of the construction of RGD-^{99m}Tc-Au PENPs.

Furthermore, the surface potential of both RGD-Au PENPs (9.13 ± 0.16 mV) and Au PENPs (12.05 ± 0.52 mV) were measured to be slightly positive after acetylation modification of the PEI amines (Table S1, Supporting Information). In addition, ultraviolet-visible (UV-vis) spectrometry was used to confirm the formation of Au NPs (Figure S2, Supporting Information), where both RGD-Au PENPs and Au PENPs possess a surface plasmon resonance (SPR) peak at 515 nm that can be assigned to the Au NPs.

Next, we used TEM to characterize the shape and size of the prepared RGD-Au PENPs and Au PENPs (Figure 1). Both particles show a round shape with a uniform size distribution. High resolution TEM images reveal that both particles are highly crystalline, as their lattice structures can be clearly discerned (see insets of Figure 1). The diameters of RGD-Au PENPs and Au PENPs were measured to be 2.6 nm and 2.2 nm, respectively, which are quite smaller than the hydrodynamic size of the corresponding particles as measured by DLS (95.7 nm for Au PENPs, and 138 nm for

8

RGD-Au PENPs, see Table S1). This is likely because only single Au core particles are measured by TEM, whereas DLS measures the clustered particles of PENPs, which may consist of many single Au NPs, in accordance with the literature.[8] What's more, the prepared RGD-Au PENPs show an excellent colloidal stability for at least 7 days after dispersion in water, PBS or cell culture medium at 4 °C (Figure S3, Supporting Information).
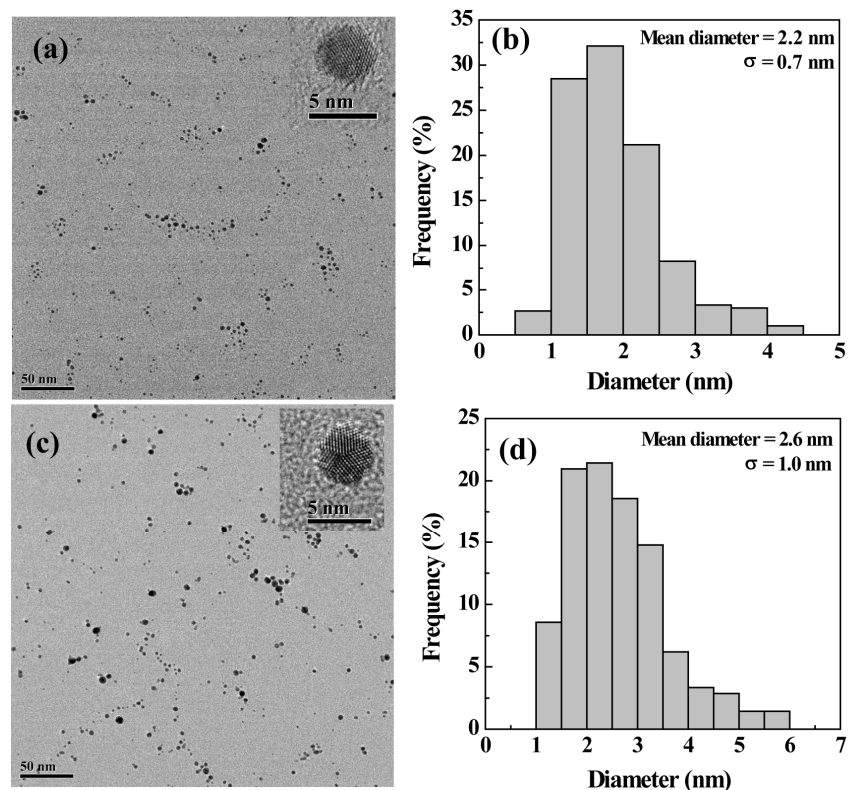

Figure 1. TEM images (a, c) and size distribution histograms (b, d) of the RGD-Au PENPs (a, b) and nontargeted Au PENPs (c, d), respectively. Inset in panels (a, c) show the high-resolution TEM images of the Au core particles of RGD-Au PENPs (a) and Au PENPs (c).

The formed RGD-Au PENPs were then labeled with ^{99m}Tc through DTPA chelation to obtain the RGD-^{99m}Tc-Au PENPs (Scheme 1). The labeling yield for the RGD-Au PENPs and Au PENPs was determined to be $71.3 \pm 4.7\%$ (n = 3) and $69.6 \pm 4.8\%$ (n = 3), respectively. The radiostability of the RGD-^{99m}Tc-Au PENPs in PBS solution was assessed by measuring the radiochemical purity of the NPs at different time periods (Figure S4, Supporting Information). Apparently, the purity of the NPs remains 99% at different storage time periods, indicating that the designed RGD-^{99m}Tc-Au

9

PENPs display a great radiostability.

X-ray Attenuation Property of the RGD-Au PENPs. We tested the X-ray attenuation property of the prepared RGD-Au PENPs to confirm their CT imaging potential (Figure S5, Supporting Information). Omnipaque was also tested for comparison. Generally, Au NPs show a better X-ray attenuation property than Omnipaque owing to the fact that Au has a higher atomic number (Z = 79) and a k-edge value (80.4 keV) than those of iodine for Omnipaque (Z = 53, 33.2 keV).[15, 51-52] As expected, the RGD-Au PENPs display a linearly increased CT contrast enhancement with the increase of Au concentration, similar to the case of Omnipaque as a function of iodine concentration. Meanwhile, the CT values of the RGD-Au PENPs are higher than that of Omnipaque under identical imaging element (iodine or Au) concentrations, particularly in relatively high concentrations of imaging element (e.g., at 0.1M, 818 HU of RGD-Au PENPs vs. 596 HU of Omnipaque), in consistence with the literature.[41-42]
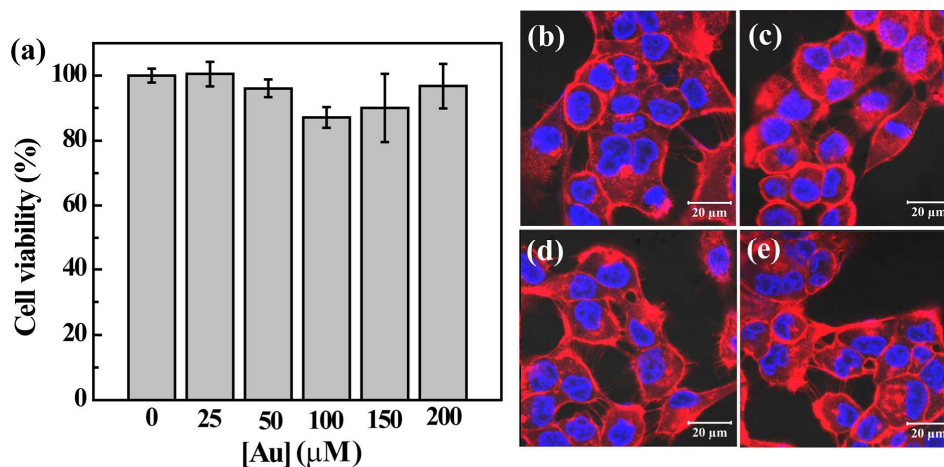
Figure 2. CCK-8 assay of HCC-LM3 cells after co-cultured with RGD-Au PENPs at the Au concentrations of 0-200 μM for 24 h (a). Confocal microscopic images of HCC-LM3 cells co-cultured with RGD-Au PENPs at the Au concentrations of 0 μM (b), 50 μM (c), 100 μM (d), and 200 μM (e), respectively for 24 h (the cytoplasm was stained with phalloidin-rhodamine, and the cell nuclei were stained with DAPI).

Cytotoxicity Assays. We used CCK-8 assay (Figure 2a) and morphology observation of cells

10

(Figure S6, Supporting Information) to evaluate the cytotoxicity of the RGD-Au PENPs. Results show that the viability and morphology of HCC-LM3 cells are pretty similar to the PBS control after the cells were co-cultured with the RGD-Au PENPs at different Au concentrations.

The cytoskeleton and nucleus of cells were also observed after being treated with RGD-Au PENPs (Figure 2b-e). The cells treated with the RGD-Au PENPs maintain the normal cytoskeleton and nucleus morphology without and cytoskeleton disruption or cellular membrane dysfunction, similar to the PBS control. Taken together, we can safely conclude that the designed RGD-Au PENPs possess an excellent cytocompatibility in the studied concentration range.
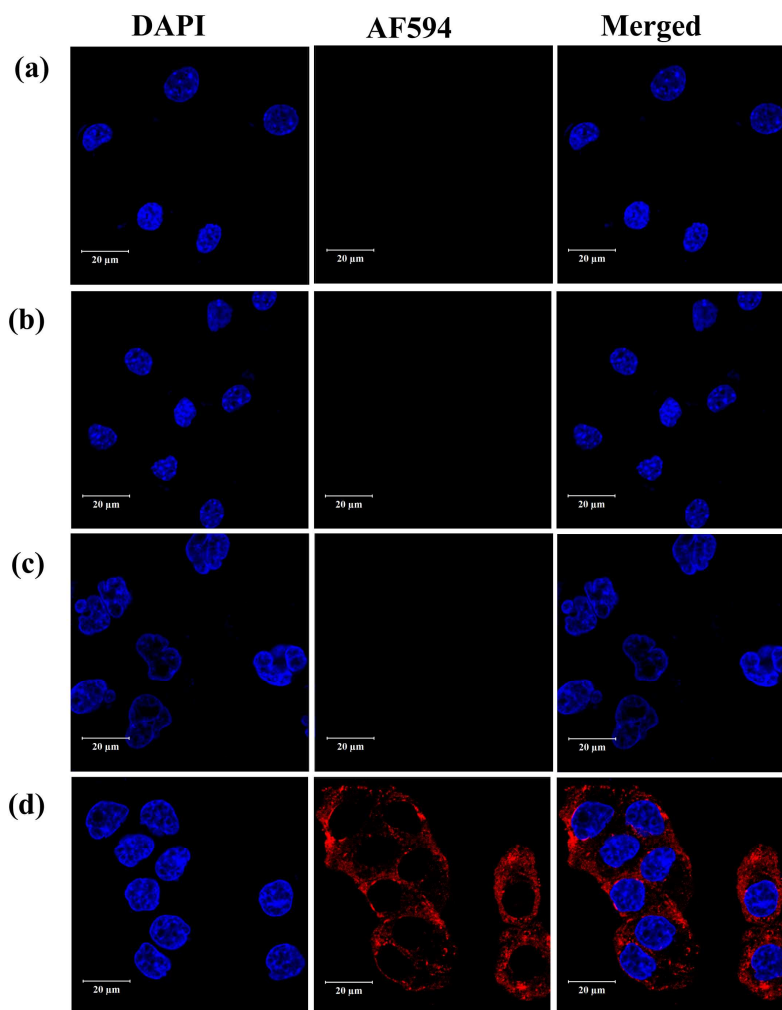

Figure 3. Immunocytochemistry of $\alpha_v\beta_3$ integrin receptor in L929 cells (negative cells; a, treated without primary antibody; b, treated with primary antibody) and HCC-LM3 cells (c, treated without primary antibody; d, treated with primary antibody). The cell nuclei were stained with DAPI, the cell membranes were stained with AF594-labeled secondary antibody.

11

Cell Immunohistochemistry. To confirm if the HCC-LM3 cells have expression of $\alpha_v\beta_3$ integrin, we performed cell immunohistochemistry assays (Figure 3). The HCC-LM3 cells treated with both primary $\alpha_v\beta_3$ integrin antibody and secondary AF594-labeled antibody display apparent red fluorescence signals (Figure 3d), which are associated to the expression of $\alpha_v\beta_3$ integrin on the surface of the HCC-LM3 cells. In sharp contrast, the negative control cells (L929 cells) treated with or without primary antibody but with the secondary antibody hardly display any red fluorescence signals (Figures 3a and 3b), suggesting that the L929 cells do not have $\alpha_v\beta_3$ integrin expression on their membranes. Moreover, the HCC-LM3 cells treated without the primary antibody do not display any red fluorescence signals even after treated with the secondary antibody (Figure 3c). These results indicate that $\alpha_v\beta_3$ integrin receptor overexpression can be found on the surface of HCC-LM3 cells. Thus, in theory, RGD-functionalized NPs should have targeting specificity to the $\alpha_v\beta_3$ integrin receptor-overexpressing cancer cells *in vitro*. It should be noted that due to the plane scanning mode of the confocal or fluorescence microscopy, in most cases, a small portion of fluorescence signals can often be found in the cytosol, even if only the cell membranes are stained, in agreement with the literature.[53-54]

Cellular Uptake. We use ICP-OES to explore whether the designed RGD-Au PENPs can be specifically taken up by hepatic carcinoma cells that overexpress $\alpha_v\beta_3$ integrin *in vitro*. As shown in Figure 4, the Au uptake by HCC-LM3 cells co-cultured with the RGD-Au PENPs is obviously higher than that co-cultured with the Au PENPs without RGD at the same Au concentrations (e.g., 4.90 ± 0.18 pg/cell for RGD-Au PENPs ([Au] = 200 μM) vs. 3.82 ± 0.17 pg/cell for Au PENPs ([Au] = 200 μM), $p < 0.01$). Furthermore, the pre-incubation of free RGD peptide with the HCC-LM3 cells leads to a much lower cellular Au uptake after incubated with the targeted RGD-Au PENPs than direct treatment of cells with the RGD-Au PENPs at the same Au concentrations. In addition, there is no significant difference in the Au uptake by HCC-LM3 cells treated with the non-targeted Au PENPs and RGD-Au PENPs with free RGD peptide cultivation at the same Au concentrations (e.g.,

12

1.94 ± 0.15 pg/cell for RGD-Au PENPs (+RGD, [Au] = 100 μM) vs. 2.00 ± 0.15 pg/cell for Au

PENPs ([Au] = 100 μM), p > 0.05). These results show that free RGD peptide is able to bind the

overexpressed $\alpha_v\beta_3$ integrin of HCC-LM3 cells, thus blocking the targeting of the RGD-Au PENPs.

This demonstrates that the formed RGD-Au PENPs are able to specifically recognize the $\alpha_v\beta_3$

integrin receptor-overexpressing cancer cells *in vitro* through receptor-mediated active targeting

effect, which is important for their applications for highly efficient tumor CT and SPECT/CT
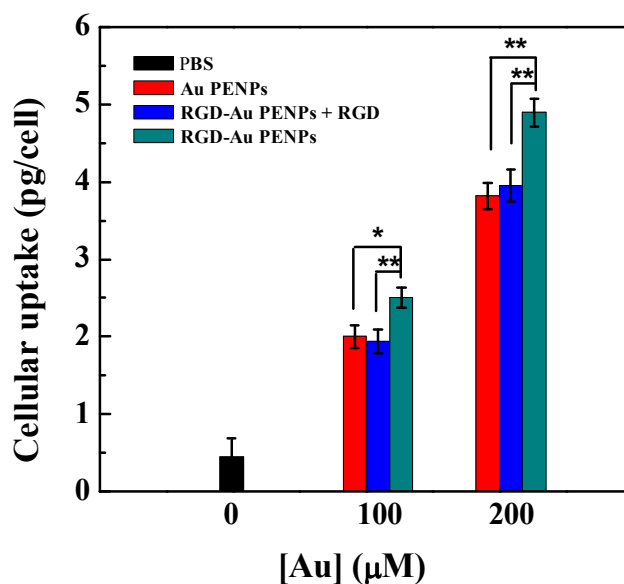
imaging.

Figure 4. Au uptake in HCC-LM3 cells treated with Au PENPs, RGD-Au PENPs (+RGD, pretreated

with free RGD peptide to block the targeting of the RGD-Au PENPs) or RGD-Au PENPs at

different Au concentrations.

CT Imaging of an Orthotopic Hepatic Carcinoma Model. CT scanning was carried out both

before and after the hepatic carcinoma bearing-mice were intravenously injected with the RGD-Au

PENPs and non-targeted Au PENPs (Figure 5). The hepatic carcinoma region shows an obvious CT

contrast enhancement after injection with these two particles (Figure 5a, and for anatomical picture

of the tumor, see Figure 5b). At 0.5 h postinjection, the tumor CT value reaches the maximum (47.1

± 1.8 HU for RGD-Au PENPs, and 32.6 ± 2.5 HU for Au PENPs), and then begins to decrease

slightly due to the metabolic process (Figure 5c). Strikingly, the tumor CT values of the mouse

13

delivered with the RGD-Au PENPs are much greater than those delivered with the non-targeted Au PENPs at the same time points (p < 0.05). In addition, the CT values of normal liver are much greater than the orthotopic hepatic carcinoma at the same time point postinjection, presumably due to the fact that these particles are mainly cleared by reticuloendothelial system (RES) located in the liver (Table S2, Supporting Information). The CT values of normal liver decrease with time postinjection, and no significance difference in CT values of normal liver can be seen after injection of the two particles (Table S2, Supporting Information). These observations imply that the RGD-functionalized Au PENPs can be efficiently taken up by $\alpha_v\beta_3$ integrin receptor-overexpressing tumor cells, resulting in enhanced orthotopic hepatic carcinoma CT imaging.
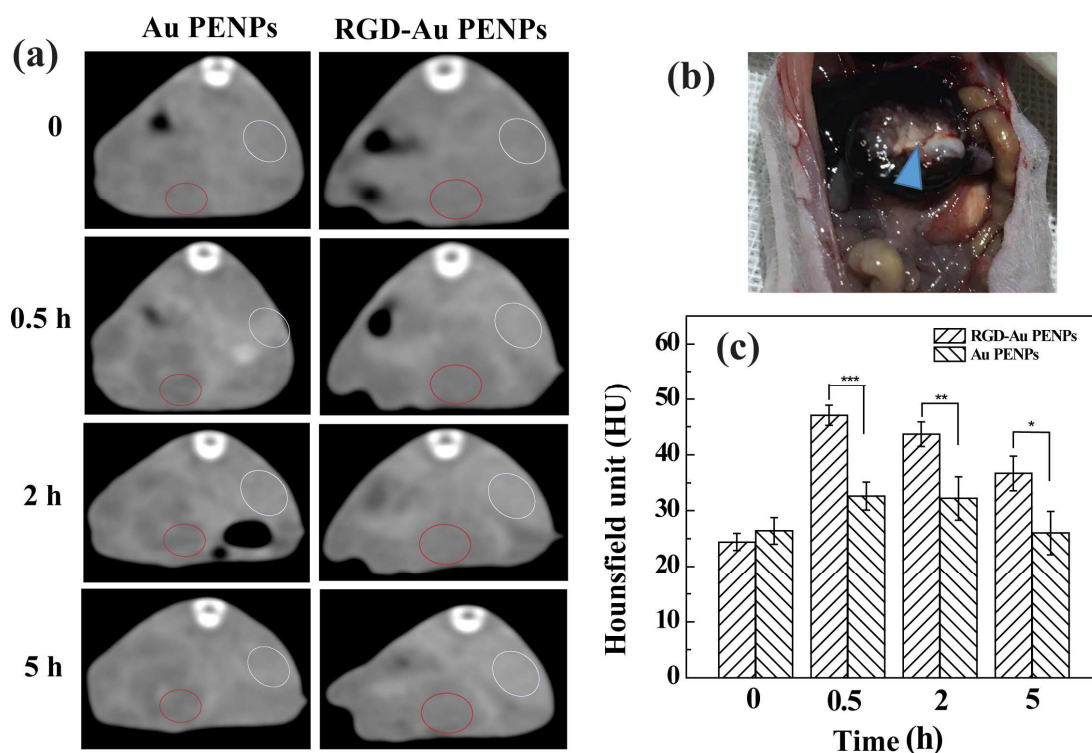
Figure 5. *In vivo* CT images (a) and CT values (c) of an orthotopic hepatic carcinoma model after intravenous administration of the RGD-Au PENPs or nontargeted Au PENPs ([Au] = 0.1 M, 150 μL PBS for each mouse) at different time points postinjection (red circle refers to the hepatic carcinoma region, white circle refers to normal liver region); (b) a photo of nude mouse bearing an orthotopic hepatic carcinoma (blue triangle refers to hepatic carcinoma region).

SPECT/CT Imaging of an Orthotopic Hepatic Carcinoma Model. Owing to the labeling of radioactive ^{99m}Tc, the formed RGD-^{99m}Tc-Au PENPs were next used for dual mode SPECT/CT imaging of an orthotopic hepatic carcinoma model. In this context, CT was just used to localize the skeleton of the mice. As shown in Figure 6a, the normal liver is much brighter than the hepatic carcinoma area (indicated with green circles) after injection, which is similar to the results of CT imaging. Moreover, the SPECT signal intensity of hepatic carcinoma region reaches the peak value (50.2 ± 0.8 μCi/mm^3 of RGD-^{99m}Tc-Au PENPs, 44.5 ± 1.3 μCi/mm^3 of ^{99m}Tc-Au PENPs) at 0.5 h postinjection of the NPs, then gradually reduces with time (Figure 6b). More importantly, RGD-^{99m}Tc-Au PENPs generated much greater SPECT signal intensity of hepatic carcinoma than the non-targeted ^{99m}Tc-Au PENPs at the same time point postinjection (Figure 6b), in accordance with the quantitative CT imaging data (Figure 5c). Our results further confirm that RGD-^{99m}Tc-Au PENPs can be more efficiently taken up by $\alpha_v\beta_3$ integrin receptor-overexpressing tumor cells in hepatic carcinoma than the non-targeted ^{99m}Tc-Au PENPs. We also find that the SPECT signal intensity of normal liver decreases with time postinjection of these two particles, and is much higher than that of the orthotopic hepatic carcinoma at the same time points, which is consistent with CT imaging data (Table S3, Supporting Information). It is interesting to note that we are attempting to highlight difference between the liver tumor region after injection of RGD-modified Au PENPs and non-targeted Au PENPs, instead to highlight the difference between the normal liver region and the liver tumor. In this case, we do not necessarily have to care about the difference of Au uptake in liver and liver tumor. In general, it is very difficult to reverse the trend that the PEGylated NPs are mainly taken up by the reticuloendothelial system (RES) and Kupffer cells of the liver and spleen,[23, 55] even though the NPs are functionalized with targeting ligands. It is also worth noting that the designed RGD-^{99m}Tc-Au PENPs are more advantageous than the commercial ^{99m}Tc-sulfur colloids (www.pharmalucence.com) in several aspects. First, our designed PEI-based nanoplatform is easily functionalized with targeted ligands to achieve specific targeting to cancer cells or can be combined with other imaging elements to realize multi-mode imaging, while ^{99m}Tc-sulfur colloid hardly

realizes multifunctionality. Second, the stability of the ^{99m}Tc-sulfur colloid may be limited in the presence of the polyvalent cations, while the RGD-^{99m}Tc-Au PENPs we prepared have a good stability in PBS. Thirdly, the ^{99m}Tc sulfur colloid is rapidly cleared by the RES from the blood with a half-life of approximately 2.5 min, while the half-life of PEGylated Au PENPs is 11.2 h,[41] which is sufficiently long for their effective uses in CT/SPECT imaging of HCC.
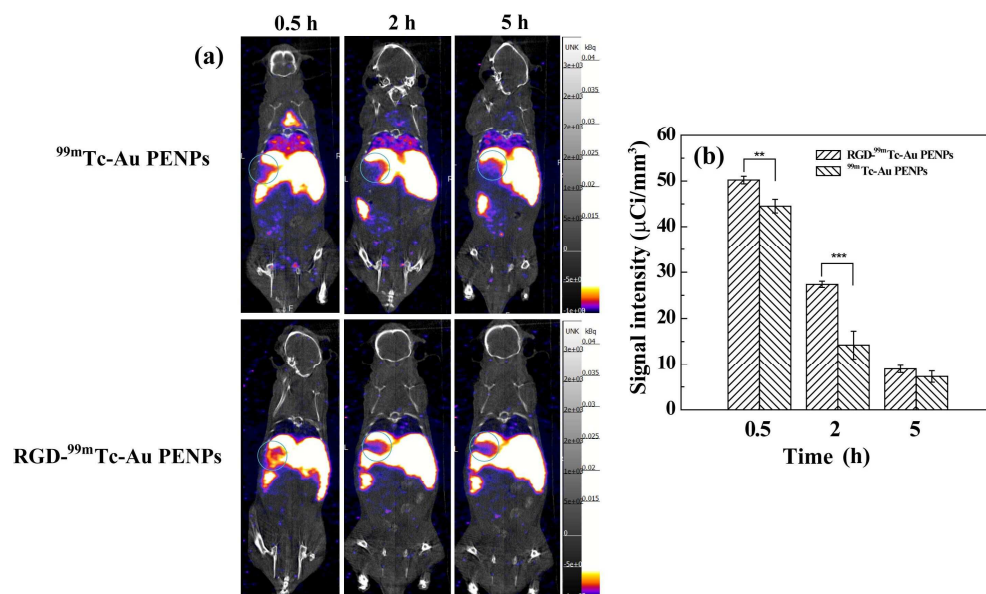

Figure 6. *In vivo* SPECT/CT images (a) and SPECT signal intensity (b) of the orthotopic hepatic carcinoma (noted as green circle) after intravenous administration of the RGD-^{99m}Tc-Au PENPs or ^{99m}Tc-Au PENPs (600 μCi ^{99m}Tc, in 150 μL PBS for each mouse) at different time points postinjection.

In Vivo **Biodistribution and Toxicity Evaluation.** To further validate the imaging results, we investigated the *in vivo* biodistribution of Au after administration of the Au PENPs (Figure S7, Supporting Information). Clearly, at 24 h postinjection, the RGD-Au PENPs are mainly taken up by spleen (1078.6 ± 121 μg/g) and liver (727.9 ± 90.1 μg/g), in accordance with the *in vivo* imaging results. In addition, no significant difference in Au uptake of organs between the RGD-Au PENPs and nontargeted Au PENPs is observed (e.g., 727.9 ± 90.1 μg/g for RGD-Au PENPs vs. 772.9 ± 78.3 μg/g for nontargeted Au PENPs in normal liver, p > 0.05). In contrast, the Au uptake in the

hepatic carcinoma region treated with the RGD-Au PENPs (310.9 ± 35.8 μg/g) is much greater than that treated with the non-targeted Au PENPs (233.1 ± 21.2 μg/g). This means that due to the RGD-mediated targeting, the developed RGD-Au PENPs can be used as a nanoprobe for enhanced tumor imaging. It should be noted that the *in vivo* biodistribution data were obtained at 24 h postinjection, whereas the SPECT/CT imaging data were collected at 5 h postinjection (for the latest time point). It is envisioned that the particles have already undergone a metabolic process at 24 h postinjection, and hence the difference between tumor uptake of the RGD-modified Au PENPs and non-targeted Au PENPs should be less, but still have a significant difference.

The long-term *in vivo* toxicity of the RGD-Au PENPs to major organs of the healthy mice was examined by H&E staining. Clearly, no histological change can be observed in the major organ slices including heart, liver, lung, spleen, and kidney at 30 days postinjection, compared with the PBS control (Figure S8, Supporting Information), demonstrating that the prepared RGD-Au PENPs possess good biocompatibility *in vivo*.

Conclusions

To conclude, we developed a versatile PEI-based nanoplatform for dual mode SPECT/CT imaging of an orthotopic tumor model. Branched PEI can be conveniently modified with DTPA to label ^{99m}Tc for SPECT imaging, entrapped with Au NPs after surface PEGylation modification for CT imaging, and be decorated with RGD peptide through a PEG spacer to endow the particles with specific targeting capacity to cancer cells expressing $\alpha_v\beta_3$ integrin *in vitro*. The designed RGD-Au PENPs with an Au core diameter of 2.6 nm are colloidally stable, cytocompatible, and can be utilized for CT imaging of the orthotopic hepatic carcinoma model. Furthermore, radioisotope of ^{99m}Tc can be efficiently labeled onto the RGD-Au PENPs *via* chelation to have desirable labelling efficiency and radiostability for highly efficient SPECT imaging of the orthotopic tumor model. The designed RGD-^{99m}Tc-Au PENPs hold a great promise to be employed as an effective nanoprobe for dual mode SPECT/CT imaging of different $\alpha_v\beta_3$ integrin receptor-overexpressing tumors.

17

Supporting Information

Additional DLS and zeta-potential data; *in vivo* CT values or SPECT signal intensity of normal liver; ^{1}H NMR; UV-vis spectra; stability assessment of RGD-Au PENPs; radiochemical purity analysis; CT images and X-ray attenuation intensity of the RGD-Au PENPs; fluorescence microscopic images of HCC-LM3 cells; *in vivo* biodistribution of the materials; and H&E staining. This material is available free of charge *via* the Internet at http://pubs.acs.org.

Acknowledgements

References

(1) El-Serag, H. B., Current Concepts Hepatocellular Carcinoma. *N. Engl. J. Med.* **2011,** *365* (12), 1118-1127.

(2) Forner, A.; Llovet, J. M.; Bruix, J., Hepatocellular Carcinoma. *Lancet* **2012,** *379* (9822), 1245-1255.

(3) El-Serag, H. B.; Rudolph, L., Hepatocellular Carcinoma: Epidemiology and Molecular Carcinogenesis. *Gastroenterology* **2007,** *132* (7), 2557-2576.

(4) Pavlov, C. S.; Casazza, G.; Semenistaia, M.; Nikolova, D.; Tsochatzis, E.; Liusina, E.; Ivashkin, V. T.; Gluud, C., Ultrasonography for Diagnosis of Alcoholic Cirrhosis in People with Alcoholic Liver Disease. *Cochrane Database Syst. Rev.* **2016,** (3), CD011602.

(5) Murakami, T.; Imai, Y.; Okada, M.; Hyodo, T.; Lee, W.-J.; Kim, M.-J.; Kim, T.; Choi, B. I., Ultrasonography, Computed Tomography and Magnetic Resonance Imaging of Hepatocellular

Carcinoma: Toward Improved Treatment Decisions. *Oncology* **2011,** *81,* 86-99.

(6) Park, W.; Chen, J.; Cho, S.; Park, S.-j.; Larson, A. C.; Na, K.; Kim, D.-H., Acidic pH-Triggered Drug-Eluting Nanocomposites for Magnetic Resonance Imaging-Monitored Intra-Arterial Drug Delivery to Hepatocellular Carcinoma. *ACS Appl. Mater. Interfaces* **2016,** *8* (20), 12711-12719.

(7) Zhao, Z.; Chi, X.; Yang, L.; Yang, R.; Ren, B. W.; Zhu, X.; Zhang, P.; Gao, J., Cation Exchange of Anisotropic-Shaped Magnetite Nanoparticles Generates Gigh-Relaxivity Contrast Agents for Liver Tumor Imaging. *Chem. Mater.* **2016,** *28* (10), 3497-3506.

(8) Liu, H.; Wang, H.; Xu, Y.; Guo, R.; Wen, S.; Huang, Y.; Liu, W.; Shen, M.; Zhao, J.; Zhang, G.; Shi, X., Lactobionic Acid-Modified Dendrimer-Entrapped Gold Nanoparticles for Targeted Computed Tomography Imaging of Human Hepatocellular Carcinoma. *ACS Appl. Mater. Interfaces* **2014,** *6* (9), 6944-6953.

(9) Hamami, M. E.; Poeppel, T. D.; Mueller, S.; Heusner, T.; Bockisch, A.; Hilgard, P.; Antoch, G., SPECT/CT with Tc-99m-MAA in Radioembolization with Y-90 Microspheres in Patients with Hepatocellular Cancer. *J. Nucl. Med.* **2009,** *50* (5), 688-692.

(10) Ilhan, H.; Goritschan, A.; Paprottka, P.; Jakobs, T. F.; Fendler, W. P.; Todica, A.; Bartenstein, P.; Hacker, M.; Haug, A. R., Predictive Value of Tc-99m-MAA SPECT for Y-90-Labeled Resin Microsphere Distribution in Radioembolization of Primary and Secondary Hepatic Tumors. *J. Nucl. Med.* **2015,** *56* (11), 1654-1660.

(11) Attarwala, A. A.; Molina-Duran, F.; Buesing, K.-A.; Schoenberg, S. O.; Bailey, D. L.; Willowson, K.; Glatting, G., Quantitative and Qualitative Assessment of Yttrium-90 PET/CT Imaging. *Plos One* **2014,** *9* (11), e0118423.

(12) Doane, T. L.; Burda, C., The Unique Role of Nanoparticles in Nanomedicine: Imaging, Drug Delivery and Therapy. *Chem. Soc. Rev.* **2012,** *41* (7), 2885-2911.

(13) Erathodiyil, N.; Ying, J. Y., Functionalization of Inorganic Nanoparticles for Bioimaging Applications. *Acc. Chem. Res.* **2011,** *44* (10), 925-935.

(14) Liang, C.; Jingjing, L.; Xing, G.; Hua, G.; Xiaoze, S.; Teng, L.; Wang, C.; Xiaoyong, W.; Gang, L.; Huaiyong, X.; Wenbo, B.; Baoquan, S.; Zhuang, L., PEGylated WS$_2$ Nanosheets as a Multifunctional Theranostic Agent for in Vivo Dual-Modal CT/Photoacoustic Imaging Guided Photothermal Therapy. *Adv. Mater.* **2014,** *26* (12), 1886-1893.

(15) Lee, N.; Choi, S. H.; Hyeon, T., Nano-Sized CT Contrast Agents. *Adv. Mater.* **2013,** *25* (19), 2641-2660.

(16) Kim, B. H.; Lee, N.; Kim, H.; An, K.; Park, Y. I.; Choi, Y.; Shin, K.; Lee, Y.; Kwon, S. G.; Na, H. B.; Park, J.-G.; Ahn, T.-Y.; Kim, Y.-W.; Moon, W. K.; Choi, S. H.; Hyeon, T., Large-Scale Synthesis of Uniform and Extremely Small-Sized Iron Oxide Nanoparticles for High-Resolution T-1 Magnetic Resonance Imaging Contrast Agents. *J. Am. Chem. Soc.* **2011,** *133* (32), 12624-12631.

(17) Lee, J. E.; Lee, N.; Kim, H.; Kim, J.; Choi, S. H.; Kim, J. H.; Kim, T.; Song, I. C.; Park, S. P.; Moon, W. K.; Hyeon, T., Uniform Mesoporous Dye-Doped Silica Nanoparticles Decorated with Multiple Magnetite Nanocrystals for Simultaneous Enhanced Magnetic Resonance Imaging, Fluorescence Imaging, and Drug Delivery. *J. Am. Chem. Soc.* **2010,** *132* (2), 552-557.

(18) Sun, C.; Lee, J. S. H.; Zhang, M., Magnetic Nanoparticles in MR imaging and Drug Delivery. *Adv. Drug Delivery Rev.* **2008,** *60* (11), 1252-1265.

(19) Sandiford, L.; Phinikaridou, A.; Protti, A.; Meszaros, L. K.; Cui, X.; Yan, Y.; Frodsham, G.; Williamson, P. A.; Gaddum, N.; Botnar, R. M.; Blower, P. J.; Green, M. A.; de Rosales, R. T. M., Bisphosphonate-Anchored PEGylation and Radiolabeling of Superparamagnetic Iron Oxide: Long-Circulating Nanoparticles for in Vivo Multimodal (T1 MRI-SPECT) Imaging. *ACS Nano* **2013,** *7* (1), 500-512.

(20) Wang, J. T.-W.; Cabana, L.; Bourgognon, M.; Kafa, H.; Protti, A.; Venner, K.; Shah, A. M.; Sosabowski, J. K.; Mather, S. J.; Roig, A.; Ke, X.; Van Tendeloo, G.; De Rosales, R. T. M.; Tobias, G.; Al-Jamal, K. T., Magnetically Decorated Multiwalled Carbon Nanotubes as Dual MRI and SPECT Contrast Agents. *Adv. Funct. Mater.* **2014,** *24* (13), 1880-1894.

(21) Kim, J.; Kim, H. S.; Lee, N.; Kim, T.; Kim, H.; Yu, T.; Song, I. C.; Moon, W. K.; Hyeon, T., Multifunctional Uniform Nanoparticles Composed of a Magnetite Nanocrystal Core and a Mesoporous Silica Shell for Magnetic Resonance and Fluorescence Imaging and for Drug Delivery. *Angew. Chem., Int. Ed.* **2008,** *47* (44), 8438-8441.

(22) Zhang, X.; Wang, H.; Wang, H.; Zhang, Q.; Xie, J.; Tian, Y.; Wang, J.; Xie, Y., Single-Layered Graphitic-C3N4 Quantum Dots for Two-Photon Fluorescence Imaging of Cellular Nucleus. *Adv. Mater.* **2014,** *26* (26), 4438-4443.

(23) Kim, D.; Park, S.; Lee, J. H.; Jeong, Y. Y.; Jon, S., Antibiofouling Polymer-Coated Gold Nanoparticles As a Contrast Agent for in Vivo X-Ray Computed Tomography Imaging. *J. Am. Chem. Soc.* **2007,** *129* (24), 7661-7665.

(24) Zhao, Y.; Pang, B.; Luehmann, H.; Detering, L.; Yang, X.; Sultan, D.; Harpstrite, S.; Sharma, V.; Cutler, C. S.; Xia, Y.; Liu, Y., Gold Nanoparticles Doped with Au-199 Atoms and Their Use for Targeted Cancer Imaging by SPECT. *Adv. Healthcare Mater.* **2016,** *5* (8), 928-935.

(25) Lee, N.; Cho, H. R.; Oh, M. H.; Lee, S. H.; Kim, K.; Kim, B. H.; Shin, K.; Ahn, T.-Y.; Choi, J. W.; Kim, Y.-W.; Choi, S. H.; Hyeon, T., Multifunctional Fe_3O_4/TaO_x Core/Shell Nanoparticles for Simultaneous Magnetic Resonance Imaging and X-Ray Computed Tomography. *J. Am. Chem. Soc.* **2012,** *134* (25), 10309-10312.

(26) Wadas, T. J.; Wong, E. H.; Weisman, G. R.; Anderson, C. J., Coordinating Radiometals of Copper, Gallium, Indium, Yttrium, and Zirconium for PET and SPECT Imaging of Disease. *Chem.*

Rev. **2010,** *110* (5), 2858-2902.

(27) Yang, Y.; Zhang, L.; Cai, J.; Li, X.; Cheng, D.; Su, H.; Zhang, J.; Liu, S.; Shi, H.; Zhang, Y.; Zhang, C., Tumor Angiogenesis Targeted Radiosensitization Therapy Using Gold Nanoprobes Guided by MRI/SPECT Imaging. *ACS Appl. Mater. Interfaces* **2016,** *8* (3), 1718-1732.

(28) Morales-Avila, E.; Ferro-Flores, G.; Ocampo-Garcia, B. E.; De Leon-Rodriguez, L. M.; Santos-Cuevas, C. L.; Garcia-Becerra, R.; Medina, L. A.; Gomez-Olivan, L., Multimeric System of Tc-99m-Labeled Gold Nanoparticles Conjugated to c RGDfK(C) for Molecular Imaging of Tumor alpha(v)beta(3) Expression. *Bioconjugate Chem.* **2011,** *22* (5), 913-922.

(29) Zhou, M.; Zhang, R.; Huang, M.; Lu, W.; Song, S.; Melancon, M. P.; Tian, M.; Liang, D.; Li, C., A Chelator-Free Multifunctional Cu-64 CuS Nanoparticle Platform for Simultaneous Micro-PET/CT Imaging and Photothermal Ablation Therapy. *J. Am. Chem. Soc.* **2010,** *132* (43), 15351-15358.

(30) Nicolas, J.; Mura, S.; Brambilla, D.; Mackiewicz, N.; Couvreur, P., Design, Functionalization Strategies and Biomedical Applications of Targeted Biodegradable/Biocompatible Polymer-Based Nanocarriers for Drug Delivery. *Chem. Soc. Rev.* **2013,** *42* (3), 1147-1235.

(31) Peer, D.; Karp, J. M.; Hong, S.; FaroKHzad, O. C.; Margalit, R.; Langer, R., Nanocarriers as an Emerging Platform for Cancer Therapy. *Nat. Nanotechnol.* **2007,** *2* (12), 751-760.

(32) Kamaly, N.; Xiao, Z.; Valencia, P. M.; Radovic-Moreno, A. F.; Farokhzad, O. C., Targeted Polymeric Therapeutic Nanoparticles: Design, Development and Clinical Translation. *Chem. Soc. Rev.* **2012,** *41* (7), 2971-3010.

(33) Veiseh, O.; Gunn, J. W.; Zhang, M., Design and Fabrication of Magnetic Nanoparticles for Targeted Drug Delivery and Imaging. *Adv. Drug Delivery Rev.* **2010,** *62* (3), 284-304.

(34) Brannon-Peppas, L.; Blanchette, J. O., Nanoparticle and Targeted Systems for Cancer Therapy. *Adv. Drug Delivery Rev.* **2004,** *56* (11), 1649-1659.

(35) Feng, L.; Yang, X.; Shi, X.; Tan, X.; Peng, R.; Wang, J.; Liu, Z., Polyethylene Glycol and Polyethylenimine Dual-Functionalized Nano-Graphene Oxide for Photothermally Enhanced Gene Delivery. *Small* **2013,** *9* (11), 1989-1997.

(36) Wang, F.; Shen, Y.; Zhang, W.; Li, M.; Wang, Y.; Zhou, D.; Guo, S., Efficient, Dual-Stimuli Responsive Cytosolic Gene Delivery Using a RGD Modified Disulfide-Linked Polyethylenimine Functionalized Gold Nanorod. *J. Controlled Release* **2014,** *196*, 37-51.

(37) Kievit, F. M.; Veiseh, O.; Bhattarai, N.; Fang, C.; Gunn, J. W.; Lee, D.; Ellenbogen, R. G.; Olson, J. M.; Zhang, M., PEI-PEG-Chitosan-Copolymer-Coated Iron Oxide Nanoparticles for Safe Gene Delivery: Synthesis, Complexation, and Transfection. *Adv. Funct. Mater.* **2009,** *19* (14), 2244-2251.

(38) Wang, G.; Huang, G.; Zhao, Y.; Pu, X.; Li, T.; Deng, J.; Lin, J., ATP Triggered Drug Release and DNA Co-Delivery Systems Based on ATP Responsive Aptamers and Polyethylenimine Complexes. *J. Mater. Chem. B* **2016,** *4* (21), 3832-3841.

(39) Zhang, G.; Gao, J.; Qian, J.; Zhang, L.; Zheng, K.; Zhong, K.; Cai, D.; Zhang, X.; Wu, Z., Hydroxylated Mesoporous Nanosilica Coated by Polyethylenimine Coupled with Gadolinium and Folic Acid: A Tumor-Targeted T-1 Magnetic Resonance Contrast Agent and Drug Delivery System. *ACS Appl. Mater. Interfaces* **2015,** *7* (26), 14192-14200.

(40) Zhou, B.; Yang, J.; Peng, C.; Zhu, J.; Tang, Y.; Zhu, X.; Shen, M.; Zhang, G.; Shi, X., PEGylated Polyethylenimine-Entrapped Gold Nanoparticles Modified with Folic Acid for Targeted Tumor CT Imaging. *Colloids Surf., B* **2016,** *140*, 489-496.

(41) Zhou, B.; Zheng, L.; Peng, C.; Li, D.; Li, J.; Wen, S.; Shen, M.; Zhang, G.; Shi, X., Synthesis and Characterization of PEGylated Polyethylenimine-Entrapped Gold Nanoparticles for Blood Pool and Tumor CT Imaging. *ACS Appl. Mater. Interfaces* **2014,** *6* (19), 17190-17199.

(42) Zhou, B.; Xiong, Z.; Zhu, J.; Shen, M.; Tang, G.; Peng, C.; Shi, X., PEGylated

Polyethylenimine-Entrapped Gold Nanoparticles Loaded with Gadolinium for Dual-Mode CT/MR Imaging Applications. *Nanomedicine* **2016,** *11* (13), 1639-1652.

(43) Hu, Y.; Yang, J.; Wei, P.; Li, J.; Ding, L.; Zhang, G.; Shi, X.; Shen, M., Facile Synthesis of Hyaluronic Acid-Modified Fe_3O_4/Au Composite Nanoparticles for Targeted Dual Mode MR/CT imaging of Tumors. *J. Mater. Chem. B* **2015,** *3* (47), 9098-9108.

(44) Hu, Y.; Li, J.; Yang, J.; Wei, P.; Luo, Y.; Ding, L.; Sun, W.; Zhang, G.; Shi, X.; Shen, M., Facile Synthesis of RGD Peptide-Modified Iron Oxide Nanoparticles with Ultrahigh Relaxivity for Targeted MR imaging of Tumors. *Biomater. Sci.* **2015,** *3* (5), 721-732.

(45) Luo, Y.; Yang, J.; Li, J.; Yu, Z.; Zhang, G.; Shi, X.; Shen, M., Facile Synthesis and Functionalization of Manganese Oxide Nanoparticles for Targeted T-1-Weighted Tumor MR Imaging. *Colloids Surf., B* **2015,** *136*, 506-513.

(46) Kong, L.; Alves, C. S.; Hou, W.; Qiu, J.; Moehwald, H.; Tomas, H.; Shi, X., RGD Peptide-Modified Dendrimer-Entrapped Gold Nanoparticles Enable Highly Efficient and Specific Gene Delivery to Stem Cells. *ACS Appl. Mater. Interfaces* **2015,** *7* (8), 4833-4843.

(47) Wen, S.; Zhao, L.; Zhao, Q.; Li, D.; Liu, C.; Yu, Z.; Shen, M.; Majoral, J.; Mignani, S.; Zhao, J.; Shi, X., A Promising Dual Mode SPECT/CT Imaging Platform Based on ^{99m}Tc-Labeled Multifunctional Dendrimer-Entrapped Gold Nanoparticles. *J. Mater. Chem. B* **2017,** *5* (21), 3810-3815.

(48) Peng, C.; Qin, J.; Zhou, B.; Chen, Q.; Shen, M.; Zhu, M.; Lu, X.; Shi, X., Targeted Tumor CT Imaging Using Folic Acid-Modified PEGylated Dendrimer-Entrapped Gold Nanoparticles. *Polym. Chem.* **2013,** *4* (16), 4412-4424.

(49) Zhou, B.; Zhao, L.; Shen, M.; Zhao, J.; Shi, X., A Multifunctional Polyethylenimine-Based Nanoplatform for Targeted Anticancer Drug Delivery to Tumors in Vivo. *J. Mater. Chem. B* **2017,** *5*

24

(8), 1542-1550.

(50) Wang, R.; Luo, Y.; Yang, S.; Lin, J.; Gao, D.; Zhao, Y.; Liu, J.; Shi, X.; Wang, X., Hyaluronic Acid-Modified Manganese-Chelated Dendrimer-Entrapped Gold Nanoparticles for the Targeted CT/MR Dual-Mode Imaging of Hepatocellular Carcinoma. *Sci. Rep.* **2016,** *6*, 33844.

(51) Guo, R.; Wang, H.; Peng, C.; Shen, M.; Zheng, L.; Zhang, G.; Shi, X., Enhanced X-Ray Attenuation Property of Dendrimer-Entrapped Gold Nanoparticles Complexed with Diatrizoic Acid. *J. Phys. Chem. C* **2011,** *21* (13), 5120-5127.

(52) Peng, C.; Zheng, L.; Chen, Q.; Shen, M.; Guo, R.; Wang, H.; Cao, X.; Zhang, G.; Shi, X., PEGylated Dendrimer-Entrapped Gold Nanoparticles for in Vivo Blood Pool and Tumor Imaging by Computed Tomography. *Biomaterials* **2012,** *33* (4), 1107-1119.

(53) Huo, T.; Du, X.; Zhang, S.; Liu, X.; Li, X., Gd-EDDA/HYNIC-RGD as an MR Molecular Probe Imaging Integrin avb3 Receptor-Expressed Tumor-MR Molecular Imaging of Angiogenesis. *Eur. J. Radiol.* **2010,** *73* (2), 420-427.

(54) Wang, H.; Zheng, L. F.; Peng, C.; Shen, M. W.; Shi, X. Y.; Zhang, G. X., Folic Acid-Modified Dendrimer-Entrapped Gold Nanoparticles as Nanoprobes for Targeted CT Imaging of Human Lung Adencarcinoma. *Biomaterials* **2013,** *34* (2), 470-480.

(55) Greish, K., Enhanced Permeability and Retention of Macromolecular Drugs in Solid Tumors: A Royal Gate for Targeted Anticancer Nanomedicines. *J. Drug Targeting* **2007,** *15* (7-8), 457-464.

Table of contents (TOC) graphic